Hydrogen–Deuterium Exchange in the Free and Immunoglobulin G-Bound Protein G B-Domain†

John Orban,* Patrick Alexander, and Philip Bryan

Center for Advanced Research in Biotechnology, University of Maryland Biotechnology Institute, 9600 Gudelsky Drive, Rockville, Maryland 20850

Received December 13, 1993; Revised Manuscript Received March 9, 1994®

ABSTRACT: Hydrogen–deuterium exchange experiments have been used to measure backbone amide proton (NH) exchange rates in the free and IgG-bound protein G B2-domain (G_{B2}). Exchange rates were analyzed in terms of the free energy required for transient opening of an H-bonded NH (ΔG_{op}), and exchange mechanisms were interpreted in the context of local and global opening motions. In free G_{B2} at 22 °C, 28 detectable NHs have ΔG_{op} values which approximate the free energy of thermal unfolding (ΔG_u) obtained from calorimetry. This indicates that the majority of detectable NHs exchange through a global unfolding mechanism, reflecting the cooperative two-state unfolding behavior observed thermodynamically [Alexander et al. (1992) *Biochemistry 31*, 3597–3603]. IgG binding results in a broadening of exchange rates and ΔG_{op} values, consistent with a less cooperative exchange mechanism than in free G_{B2}. The large range of protection factors (1.3 to >210) also indicates that exchange does not occur cooperatively for all detectable NHs in bound G_{B2}. Nineteen of the detectable NHs have significantly slowed exchange rates in the complex with protection factors >5. Residues with protection factors of the order of 100 or more occur in both the helix region (F30, K31, A34) and in the central core of the β-sheet (V6, F52, V54). The highest protection factors are consistent with a binding constant of $\sim 10^8$ M^{-1}. The pattern of high protection observed in the helix overlaps with the putative binding site suggested from previous studies. However, the highly protected residues in the central core of the β-sheet are removed from the putative binding interface. This suggests that IgG binding affects conformational dynamics in G_{B2}. The highly protected residues, which are mostly buried from the solvent-accessible surface, constitute the slow-exchange core of bound G_{B2} and most likely exchange as a cooperative unit by global unfolding. Thus, the rigid slow-exchange core probably corresponds with the folding core of the bound protein. Residues with intermediate protection factors are situated further out from the slow-exchange core, and the smallest protection factor residues are near the surface or at the ends of β-strands. These latter residues can exchange in the complex without complete unfolding of bound G_{B2}. While these locally unfolded states are still energetically costly, they do not greatly disrupt IgG binding. However, globally unfolded states are not consistent with binding to IgG.

Mapping of antigenic sites on proteins using hydrogen–deuterium (H–D) exchange was first described by Paterson et al. (1990). The basic principle is that main-chain amide protons (NHs) which are buried on protein–protein complex formation have slowed exchange rates when compared with the free protein (Brandt & Woodward, 1987; Werner & Wemmer, 1992; Zinn-Justin et al., 1993). The method used by Paterson et al. (1990) involved immobilization of the larger protein, an antibody, on a polymer support. The smaller protein, horse cytochrome *c*, was bound to the immobilized antibody and incubated in a deuterated buffer system. After a specified time, exchange was quenched, the small protein eluted, and the degree of H–D exchange for individual NHs determined by 2D NMR spectroscopy. In this way, the antibody binding site was imprinted on the smaller protein and measured indirectly, thus avoiding the problem of analyzing a high molecular weight complex directly. The binding site determined from H–D exchange for cytochrome *c* was found to be consistent with prior epitope mapping studies.

Recent studies have shown that some NHs outside the structural epitope can also have significantly slowed exchange behavior (Mayne et al., 1992; Benjamin et al., 1992). In the complex between hen egg lysozyme and the antibody HyHEL-5, a number of NHs remote from the crystallographic binding interface were also significantly protected (Benjamin et al., 1992). These results suggest that antibody binding can have an effect on the conformational dynamics of the antigen.

In this paper, we report exchange rate measurements in the free and immunoglobulin G- (IgG-) bound protein G B2-domain (denoted here as G_{B2}) using the H–D exchange method of Paterson et al. (1990). Protein G is a multidomain component of the cell wall of streptococcal species of the Lancefield group G and binds to all subclasses of human IgG by the constant Fc region (Myhre & Kronvall, 1977; Reis et al., 1984). Binding to the Fab fragment has also been observed. Protein G is organized into functional domains similar to those of staphylococcal protein A (Åkerstrom & Bjorck, 1986), and the IgG binding domains are similar in size. These domains have been shown to consist of two or three repeats of 55 amino acids separated by about 15 unique amino acids (Fahnestock et al., 1986). Protein G and protein A compete for binding at a site on the C_{H2}–C_{H3} interface of IgG (Wright et al., 1977; Stone et al., 1989). No homology exists, however, between the IgG binding domains of protein A and protein G on the levels of either primary sequence or tertiary structure. The protein A structure consists of a three-helix bundle (Gouda et al., 1992). In contrast, the global fold of the 55 amino acid domains of protein G consists of a four-stranded β-sheet spanned by a helix as depicted in Figure 1 (Gronenborn et al., 1991; Lian et al., 1991, 1992; Orban et al., 1992). While the

† Supported by NSF Grant MCB-92-19309.
* Author to whom correspondence should be addressed.
® Abstract published in *Advance ACS Abstracts,* April 15, 1994.

0006-2960/94/0433-5702$04.50/0

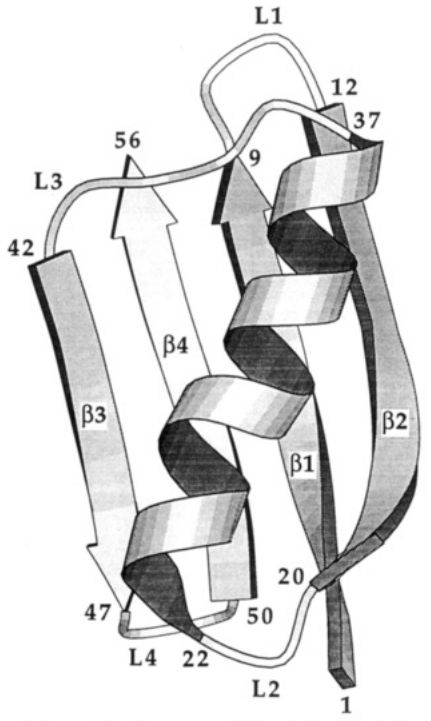

FIGURE 1: Schematic diagram of the global fold for protein G (Gronenborn et al., 1991) generated using MOLSCRIPT (Kraulis, 1991).

crystal structure of the protein A–Fc complex has been determined (Deisenhofer, 1981), no detailed structural information has been available to date on the protein G–Fc complex. However, peptide mapping (Frick et al., 1992) and chemical shift perturbation experiments (Gronenborn & Clore, 1993) implicate the helix and β3-strand of protein G in binding to IgG.

Here, exchange rates in free and bound G_{B2} are analyzed in terms of the structural unfolding model, in which the mechanism of exchange can be described by the reaction path (Hvidt & Nielsen, 1966)

$$F(H) \underset{k_f}{\overset{k_u}{\rightleftharpoons}} U(H) \xrightarrow[D_2O]{k_c} U(D) \underset{k_u}{\overset{k_f}{\rightleftharpoons}} F(D) \qquad (1)$$

where k_u, k_f, and k_c are the unfolding, folding, and intrinsic exchange rates, respectively, F is the native or folded state, and U represents open or unfolded states. Since stabilizing conditions more than 50 °C below the T_m were used ($k_f \gg k_u$), and $k_f \gg k_c$ (EX_2 limit), the measured exchange rate, k_{ex}, is given by

$$k_{ex} = k_u k_c / k_f = K_{op} k_c \qquad (2)$$

The free energy required for transient opening is then

$$\Delta G_{op} = -RT \ln K_{op} = -RT \ln(k_{ex}/k_c) \qquad (3)$$

where K_{op} is the equilibrium constant for transient opening and ΔG_{op} is the free energy difference between folded and locally or globally unfolded states.

The ΔG_{op} values from NH exchange are compared with the calorimetric free energy of thermal unfolding, ΔG_u, and exchange mechanisms in free and bound G_{B2} are discussed. We show that IgG binding appears to affect dynamics in G_{B2} such that a number of distal NHs are as highly protected from exchange as NHs buried at the putative binding interface. These results are discussed in the context of local and global opening motions in bound G_{B2}.

MATERIALS AND METHODS

IgG-Binding Experiments. The protein G B2-domain was cloned, expressed, and purified as described in Alexander et al. (1992). pH measurements in D_2O (pD) were uncorrected and refer to direct meter readings. A typical binding experiment was carried out in the following manner. A slight excess of G_{B2} (~13 mg) was loaded onto a column of total human IgG–Sepharose (Pharmacia, 5-mL resin volume) in 5–10 mL of phosphate-buffered saline (50 mM K_2HPO_4/KH_2PO_4, 150 mM NaCl, pH 7.0) at 3 °C (cold room), followed by extensive washing (25 mL) to remove unbound G_{B2}. The column was then washed thoroughly with the corresponding deuterated phosphate-buffered saline (pD 7.0, 25 mL) and incubated at 3 °C for 1, 3, 27, 81, or 243 h. Additional experiments were carried out at 22 °C with incubation times of 2, 9, and 18 h. The H–D exchange was quenched by washing the column with 5 mM deuterated ammonium acetate/D_2O (Cambridge Isotope Laboratories) (pD 5.0, 25 mL), conditions which minimized further exchange but did not disrupt the IgG–G_{B2} complex. G_{B2} was eluted from the support with 0.5 M deuterated ammonium acetate/D_2O solution (pD 3.0, 25 mL) to provide samples with a final pD ~3.6. Samples were lyophilized and then ready for analysis by NMR. Control experiments were carried out by first incubating G_{B2} (~13 mg) in deuterated phosphate buffer (pD 7.0, 1.65-mL approximate void volume of column) for a specified time, then loading the sample onto an IgG–Sepharose column, rapidly lowering the pD to 5.0, and eluting as described above. Fresh samples of G_{B2} were used for each H–D exchange time point. After each experiment, the IgG–Sepharose column was washed with 1 M acetic acid solution to remove any residual G_{B2} from the column and then with phosphate-buffered saline until the eluent was back to pH 7. A single column was used for all the binding and control experiments.

NMR Spectroscopy. NMR samples were prepared by dissolving lyophilized protein in 0.4 mL of 99.99% D_2O containing 100 mM NaOAc-d_3 at pH 5.4. Sample concentrations were ~5 mM, and chemical shifts were referenced to external sodium 2,2-dimethyl-2-silapentane-5-sulfonate (DSS). All NMR spectra were recorded at 25 °C on a Bruker AMX-500 spectrometer and processed on a Silicon Graphics 4D/35 workstation using FTNMR and FELIX (Hare Research Inc., Bothell, WA). NOESY (Jeener et al., 1979; Kumar et al., 1980) experiments were acquired in the hypercomplex mode (States et al., 1982) with standard phase-cycling schemes. The mixing time was 120 ms with up to 10% random variation to suppress zero quantum coherence (Macura et al., 1981). All two-dimensional experiments were recorded with 1024 complex points in t_2 and 400 increments in t_1 with a spectral width of 6024 Hz in both dimensions. For each t_1 value, eight transients were collected with a relaxation delay of 2.0 s between scans. No solvent suppression methods were employed since the residual HOD signal was minimal. NOESY spectra were recorded immediately after dissolution in D_2O. A standard G_{B2} sample in D_2O was used to shim the magnet prior to insertion of H–D exchanged samples. The total data collection time for each sample, starting with the addition of D_2O, was 4.5 h.

NOESY spectra were multiplied in t_2 by a window function with a value of 1.0 for the first 256 points which dropped smoothly to zero at 1024 points as a sine-bell squared function. In the t_1 dimension, NOESY data were multiplied with a 90°

Table 1: Exchange Rates (h^{-1}) for the Main-Chain Amide Protons of G_{B2} at pH 7.0, 3 and 22 °C

	T = 3 °C					T = 22 °C				
residue	k_f	k_b	P_{lo}	P_{av}	P_{hi}	k_f	k_b	P_{lo}	P_{av}	P_{hi}
Tyr3	0.010	0.0084	1.1	1.2	1.3	0.26	0.14	1.1	1.9	2.9
Lys4	0.0035	<0.001	3.1	>3.5	>3.9	0.21	0.013	15	16	19
Leu5	0.0019	<0.001	>1.5	>1.9	>2.9	0.15	0.0044	21	34	100
Val6	0.0012	<0.001	>1.0	>1.2	>1.3	0.11	<0.0012	>87	>92	93
Ile7	0.0135	0.0055	2.4	2.45	2.5	0.22	0.059	3.6	3.7	3.9
Asn8[a]	0.010	0.0040		2.5		0.17	0.066		2.6	
Thr18[b]	0.50	0.093	4.1	5.4	6.7					
Ala20	0.010	0.0025	2.6	4.0	6.0	0.28	0.060	3.3	4.7	6.7
Ala26	0.0053	<0.001	>4.4	>5.3	>6.1	0.27	0.020	8.9	14	25
Glu27	0.0025	<0.001	>1.8	>2.5	>3.5	0.16	0.022	6.4	7.3	9.4
Lys28	0.0098	0.0019	3.8	5.2	6.7	0.24	0.045	3.0	5.3	11
Ala29[a]	0.0091	0.0051		1.8		0.24	0.14		1.7	
Phe30	0.0017	<0.001	>1.4	>1.7	>2.0	0.14	<0.0018	43	>78	>140
Lys31	0.0016	<0.001	>1.0	>1.6	>2.0	0.16	<0.0014	65	>110	>190
Gln32	0.0087	0.0063	1.2	1.4	1.5	0.18	0.095	1.7	1.9	2.2
Tyr33	0.013	<0.001	>11	>13	>16	0.28	0.017	14	16	24
Ala34	0.010	<0.001	>8.6	>10	>13	0.25	<0.0012	170	>210	>280
Asn35	0.0070	<0.0011	5.9	>6.4	>7.5	0.11	0.013	7.9	8.5	10
Asp36	0.0071	0.0021	3.0	3.4	3.7	0.13	0.047	2.3	2.8	3.0
Asn37	0.0050	0.0035	1.3	1.4	1.5	0.12	0.056	1.2	2.1	4.4
Val39	0.0074	<0.001	>5.9	>7.4	>10	0.11	0.0049	15	22	53
Val42	0.0085	0.0021	3.6	4.0	4.4	0.17	0.033	4.4	5.2	5.8
Thr44	0.0020	<0.001	>1.0	>2.0	>3.8	0.15	0.014	6.1	11	15
Asp46	0.0023	0.0024	0.76	1.0	1.3	0.14	0.053	1.7	2.6	4.0
Lys50	0.0070	0.0053	1.3	1.32	1.4	0.14	0.072	1.9	1.94	2.0
Thr51	0.0018	<0.001	>1.8	>1.8	>1.8	0.19	0.019	9.5	10	11
Phe52	0.0015	<0.001	>1.0	>1.5	>2.0	0.18	<0.001	>160	>180	>190
Thr53	0.0013	<0.001	>1.0	>1.3	>1.8	0.16	0.0068	18	24	38
Val54	0.0011	<0.001	>1.0	>1.1	>1.2	0.13	<0.0018	52	>72	>130
Thr55	0.0035	0.0012	2.3	2.9	4.0	0.13	0.027	4.4	4.8	5.4
Glu56	0.0055	0.0053	0.85	1.0	1.4	0.15	0.12	1.2	1.3	1.4

[a] Data obtained from one cross-peak. [b] Not observed at 22 °C.

shifted sine-bell squared function of 400 points. For all two-dimensional data, the first t_1 experiment was multiplied by 0.5 to suppress t_1 ridge noise (Otting et al., 1985).

Determination of Amide Proton Exchange Rates. Specific amide proton exchange rates in free G_{B2} (k_{free}) and in the G_{B2}–IgG complex (k_{bound}) were determined by integration of NOESY cross-peaks such as αCH(i)-NH(i) and βCH(i)–NH(i) at each time point, depending on the degree of peak overlap. In cases where these cross-peaks were too overlapped, alternative resolvable cross-peaks such as α, β, or γCH(i–1)–NH(i) connectivities were used. Four well-resolved cross-peaks due to nonlabile protons, βCH(30)–δCH(30), αCH(17)–βCH(17), αCH(33)–δCH(33), and βCH(45)–δCH(52), were integrated, and the average volume was used to normalize peak volumes between time points. The zero time point for normalized peak intensity at 3 °C was used as the zero time point for the 22 °C data. Estimated errors in peak volume integrals were obtained by integration of the noise level near the relevant cross-peak and were in the range 5–15% of the peak integral. Plots of normalized peak volume versus time were fitted to a single exponential decay, and exchange rates were determined from the slope of ln(peak volume) versus time.

Random coil intrinsic exchange rates were calculated using procedures previously discussed (Englander et al., 1979; Roder et al., 1985; Robertson & Baldwin, 1991). Values used for the acid- and base-catalyzed rate constants at 0 °C were $k_{D^+} = 5.78 \times 10^{-2}$ M^{-1} s^{-1} and $k_{OD^-} = 4.33 \times 10^{8}$ M^{-1} s^{-1}, respectively (Roder et al., 1985). These rates were corrected for each main-chain amide group on the basis of the nearest-neighbor side chains (Molday et al., 1972). Exchange rates at 0 °C were extrapolated to 3 °C and 22 °C using the activation enthalpies $\Delta H^{\ddagger}_{D^+}$ = 15 kcal mol^{-1} and $\Delta H^{\ddagger}_{OD^-}$ = 2.6 kcal mol^{-1} (Englander & Poulsen, 1969). The temperature dependence of the water dissociation constant was accounted for using the relationship determined by Covington et al. (1966).

RESULTS

Amide Proton Exchange Rates in Free G_{B2}. Assignments of amide proton resonances were obtained from previous work (Orban et al., 1992). For a given residue, the amide proton exchange rate was generally obtained from more than one resolvable NOESY cross-peak and averaged. A complete list of exchange rates obtained for each cross-peak is provided in supplementary Table 1. NOESY spectra provided the option of using a number of alternative well-resolved NOE cross-peaks for the determination of exchange rates [cf. Werner and Wemmer (1992)]. For some NHs, the diagonal peaks were also sufficiently well resolved to be integrated.

Exchange rates in free G_{B2} were obtained for 30 of the 55 main-chain NHs at 22 °C. At 3 °C, an additional NH resonance due to T18 could also be detected. Among H-bonded NHs, resonances due to G9, L12, G14, T16, and G38 were undetectable using the H–D exchange method described here. The non-H-bonded NHs exchanged too quickly to be detected using this method.

The 30 slowest exchanging H-bonded NHs have rates which are clustered within an order of magnitude of each other at both 3 and 22 °C (Table 1). The variations in k_{free} observed within this range are generally correlated with the overall secondary and tertiary structure of G_{B2} (Figure 2). In the parallel-stranded β-sheet region, exchange rates are generally higher at the ends of each strand than in the center. For example, in the β1-strand Y3 and G9 have faster exchange rates than the central residues L5 and V6. Similar observations can be made for the β4-strand though the differences are

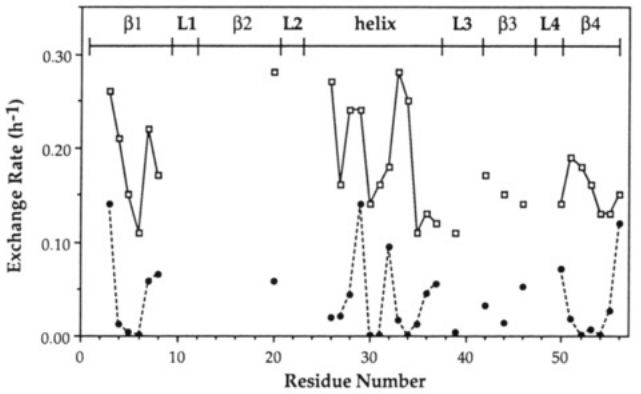

FIGURE 2: Plots of k_{free} (open squares) and k_{bound} (closed circles) at 22 °C vs residue number. Values for (i)–$(i+1)$ nearest neighbors are connected by solid lines (k_{free}) or dashed lines (k_{bound}).

smaller. The rapid exchange of the NHs of L12, G14, T16, and T18 suggests that the β2-strand is distorted or somewhat more flexible than other strands forming the β-sheet. This is consistent with the NOE data for G_{B2} (Orban et al., 1992; Lian et al., 1992).

In the helix, 11 H-bonded main-chain NHs can be detected corresponding to residues 26–37, and these rates appear to have a periodicity which parallels burial of NHs from the solvent-accessible surface for some residues. For example, the NH of F30 is buried and has a slower exchange rate than the surface NHs of K28 and Y33. However, a number of other NHs do not fit into this pattern. Most notably, A34NH is buried but has one of the fastest exchange rates of the set of detectable NHs.

The loop structure connecting the helix to the β3-strand, L3, consists of a short extended chain conformation involving residues G38, V39, D40, and G41. The NH of G38 exchanges too quickly to be observed. However, the NH of V39 forms an H-bond with the main-chain carbonyl oxygen of A34 (Gronenborn et al., 1991) and exchanges slowly in D_2O. The remaining L3 residues, D40 and G41, do not appear to have H-bonded NHs, and exchange rates could not be obtained for these residues using the H–D exchange method. The main-chain NHs in L1, L2, and L4 also exchange too quickly to be observed with the exception of K50, which forms an H-bond with D46.

Using eq 3, ΔG_{op} was calculated for detectable NHs at 3 and 22 °C. At 22 °C, ΔG_{op} values were clustered about a mean value of 7.2 ± 0.5 kcal mol^{-1}, where the range is ±1 standard deviation (Figure 3A). The range of ΔG_{op} observed is quite narrow, as expected for a set of NHs with similar exchange kinetics. The only exception is E56NH, which is at the C-terminus of the main chain and has a ΔG_{op} value of 5.6 kcal mol^{-1}. The ΔG_{op} values for buried NHs such as L5, V6, F30, A34, F52, and V54 are within 1 kcal mol^{-1} of those for surface NHs such as K28, Q32, and Y33. Similar results were observed at 3 °C (data not shown). Comparison of these values with the free energy of thermal unfolding (ΔG_u) from differential scanning calorimetry (DSC; Alexander et al., 1992) is summarized in Table 2.

Amide Proton Exchange Rates and Protection Factors in the IgG–G_{B2} Complex. Figure 4 shows part of the NOESY fingerprint region for free and bound G_{B2} and demonstrates the effects of IgG binding on NH exchange. Representative binding curves are shown in Figure 5.

At 3 °C, exchange rates in the complex were too slow for precise measurement for 16 of the 31 detectable NHs, with $k_{bound} < 0.001$ h^{-1}. At 22 °C, values for k_{bound} were spread

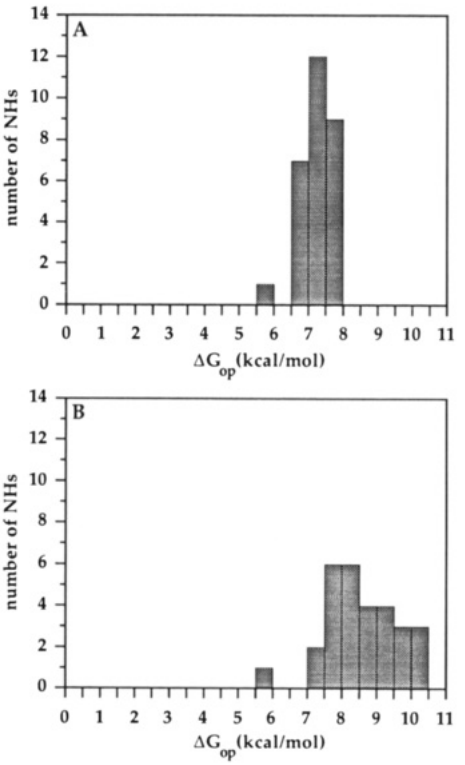

FIGURE 3: Histogram representation of the range of ΔG_{op} values for detectable NHs at 22 °C vs the number of NHs in each range for (A) free G_{B2} and (B) bound G_{B2}. In both graphs, the lowest ΔG_{op} value obtained was for the NH of the C-terminal residue, E56.

Table 2: Free Energies of Unfolding from NH Exchange[a] and Calorimetric Data

	T = 3 °C	T = 22 °C
ΔG_{op} (NH exchange)[b]	7.7 ± 0.7	7.3 ± 0.5
ΔG_{op} (NH exchange)[c]	6.6 ± 0.5	6.1 ± 0.5
ΔG_u (DSC)[d]	6.3 ± 0.5	6.1 ± 0.5

[a] Mean values (±1 standard deviation) are for the clustered set of ΔG_{op} values at 3 and 22 °C and do not include T18 and E56. [b] Calculated using correction factors from Molday et al. (1972). [c] Calculated using correction factors from Bai et al. (1993). [d] Extrapolated from thermal unfolding data at pH 5.4 (see text; Alexander et al., 1992).

over more than a factor of 100, compared with a factor of 2–3 in the range of k_{free} values (Figure 6). This corresponds to an increase and broadening of ΔG_{op} values (Figure 3B). No observable NHs exchanged faster upon complex formation, indicating no gross conformational change in G_{B2} on binding to IgG.

Protection factors were obtained at 3 and 22 °C and are quoted as average values, P_{av} [$=k_{free}(av)/k_{bound}(av)$] (Table 1). In addition, the lower and upper limits of the range of P values observed for each residue are given as P_{lo} and P_{hi}, respectively. These values provide an estimate of errors in the measurement of protection factors. For most NHs, P_{hi} is within a factor of 3 of P_{lo}. Protection factors are summarized graphically in Figure 7. Where small enough for comparison, protection factors for a given residue at 3 and 22 °C were within experimental error.

All detectable NH protons were protected to varying degrees with protection factors ranging from 1.3 to >210. Nineteen of the detectable NHs have $P > 5$ at 22 °C. Some exchange rates in complexed G_{B2} were too slow to be measured for a number of NHs, even at 22 °C. These correspond to the most strongly protected NHs, which are V6 in the β1-strand; F30, K31, and A34 in the helix; and F52 and V54 in the β4-strand.

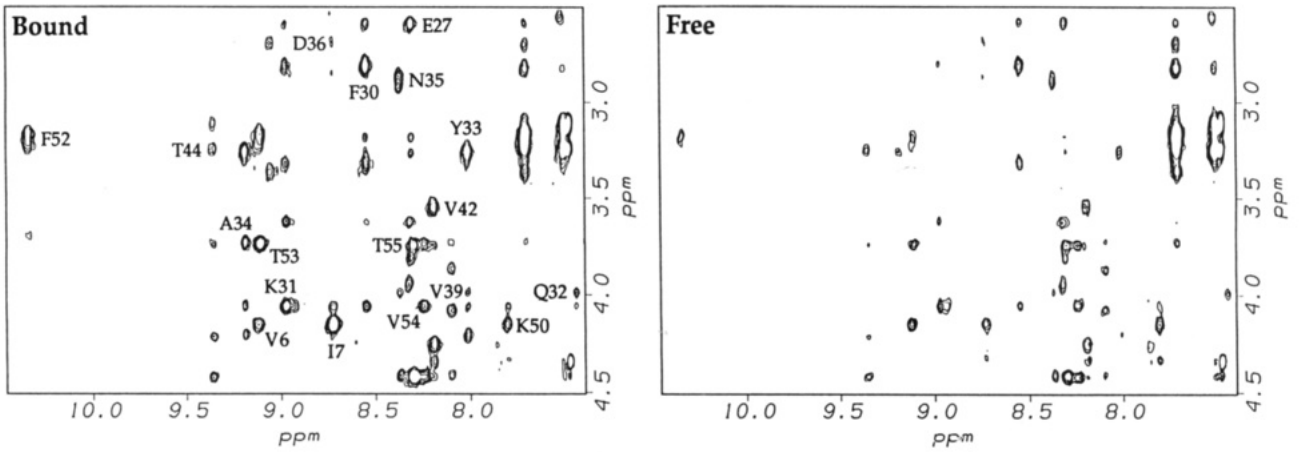

FIGURE 4: Part of the NOESY fingerprint region for the 9-h time point at 22 °C in IgG-bound G_{B2} (left) and free G_{B2} (right). Labeled peaks show αCH(i)–NH(i) connectivities for residues 6, 27, 31, 32, 34, 39, and 50; for residues 33, 35, 36, 52, 53, and 55, the βCH(i)–NH(i) connectivities are shown. Other labeled cross-peaks are αCH(i–1)–NH(i) correlations for residues 7 and 42, βCH(i–1)–NH(i) for residue 44, and 7αCH–54NH for residue 54.

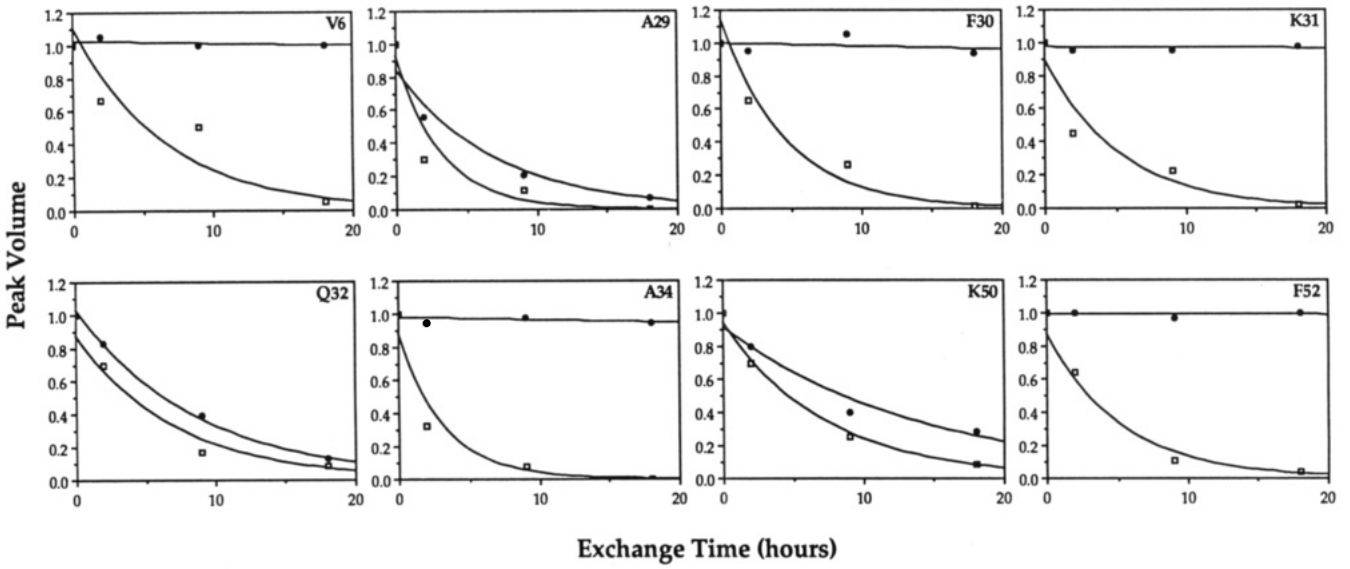

FIGURE 5: Representative plots of normalized peak volume vs exchange time in free G_{B2} (open squares) and IgG-bound G_{B2} (closed circles). Values shown were obtained from αCH(i)–NH(i) cross-peaks, except for residues 30 and 31 where βCH(i)–NH(i) and γCH(i)–NH(i) cross-peaks were used, respectively.

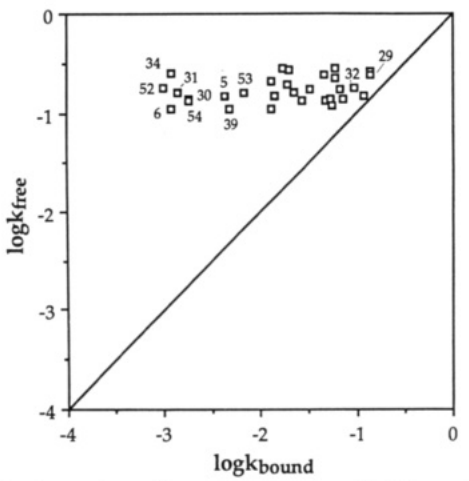

FIGURE 6: Comparison of k_{free} and k_{bound} values (h^{-1}) for each residue (open squares) at 22 °C. Residues with the highest protection factors are furthest from the diagonal while residues with small protection factors are close to the diagonal.

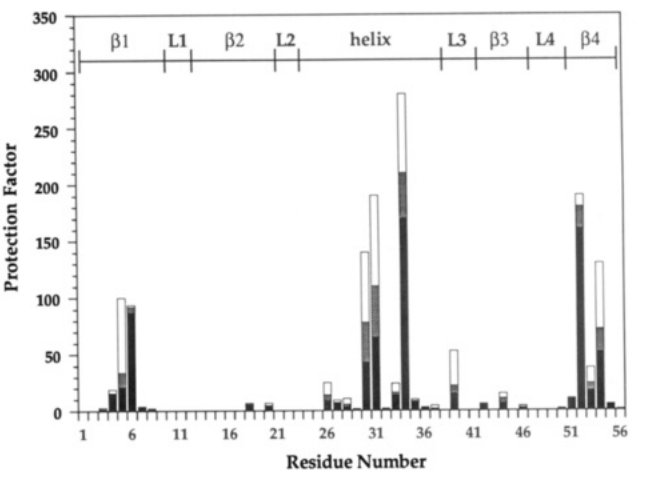

FIGURE 7: Summary of protection factors at 22 °C as a function of residue number showing values of P_{av} (hatched bars), P_{lo} (filled bars), and P_{hi} (open bars). The values for T18 are from 3 °C binding experiments.

Other residues with high protection factors ($P > 20$) are L5, V39, and T53. The protection factors were mapped onto the three-dimensional structure of protein G (Figure 8), and a number of observations were made regarding the pattern of slowed exchange. First, highly protected residues with protection factors of the order of 100 or more occur in both

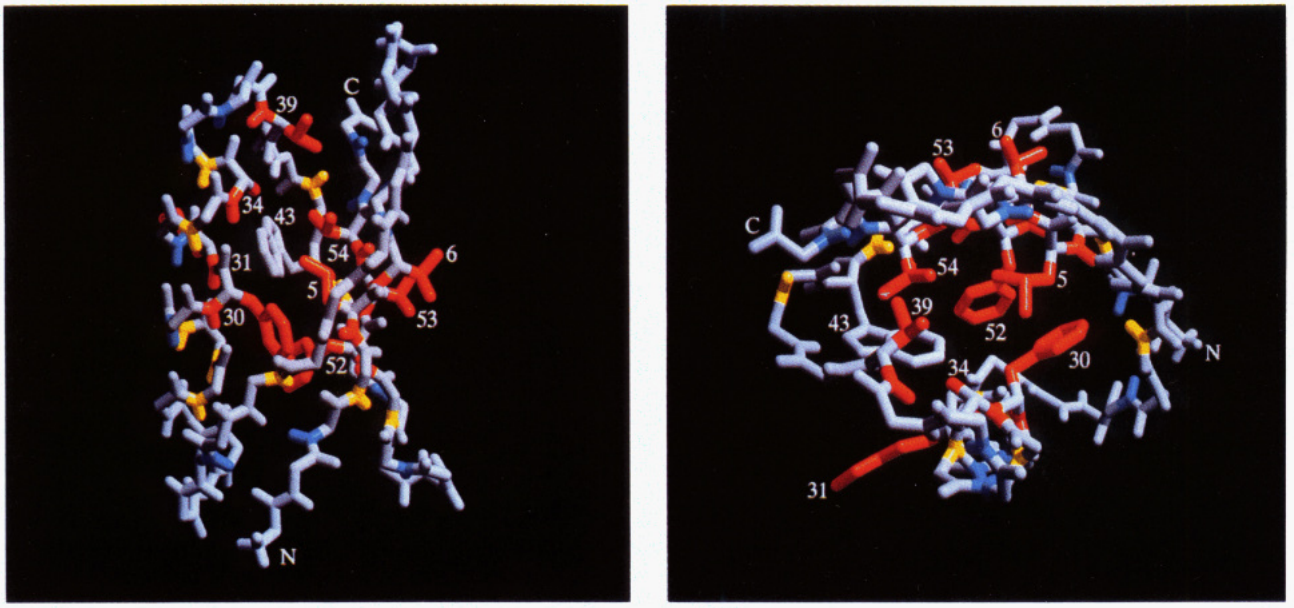

FIGURE 8: Two views of the protein G structure (Gronenborn et al., 1991) showing main-chain amide protons protected from exchange in the complex with IgG. Amide protons with $P < 5$ are in blue and those with $P > 20$ are in red. Those with intermediate P values are in yellow. Side chains of residues with $P > 20$ are also shown in red. The right panel shows the view from the C-terminal end of the helix. The diagrams were generated using RASTER3D (D. Bacon, Center for Advanced Research in Biotechnology).

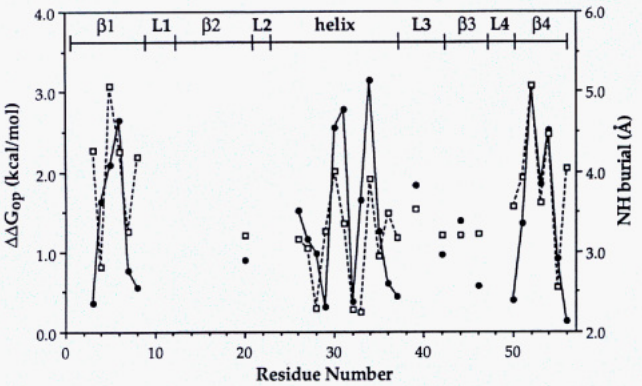

FIGURE 9: Comparison of $\Delta\Delta G_{op}$ values (filled circles) and NH burial (open squares) as a function of residue number. The NH burial is the depth (in Å) of the backbone amide hydrogen atom center from the solvent-accessible surface of protein G (Gronenborn et al., 1991) as calculated using the program SURANA (J. Moult, Center for Advanced Research in Biotechnology). Van der Waals radii used were from Chothia (1976). A radius of 1.0 Å was used for amide hydrogen atoms, and a probe radius of 1.4 Å was used for water molecules.

the helix region (F30, K31, A34) and in the central core of the β-sheet (V6, F52, V54). Thus, no single contiguous binding surface is apparent from this pattern of protection factors. Second, the majority of the highly protected NHs are also among the most buried from the solvent-accessible surface of free G_{B2}. The degree of protection from exchange can be expressed in terms of $\Delta\Delta G_{op}$ [$=\Delta G_{op}$(bound) – ΔG_{op}(free)], where the free energy difference is largest for NHs which are most protected from exchange in the complex. The most highly protected NHs have lower limit values of $\Delta\Delta G_{op} > 2.5$ kcal mol^{-1}. With the exception of K31NH, all of these are buried more than ~4 Å from the solvent-accessible surface (Figure 9).

In the β-sheet, protection from exchange is strongest in the core of the sheet at the central residues of the β1- (L5, V6) and β4-strands (F52, T53, V54) with progressively weaker protection at the outer residues of these strands. In contrast, H-bonded NHs in the β3-strand have only moderately slowed exchange rates, with protection factors ranging from 2.6 to 11. Limited information can be obtained for the β2-strand since L12, G14, and T16 exchange too quickly to be detected using the H–D exchange methods employed here. However, T18 and A20 also have only moderate protection factors of 5.4 and 4.0, respectively, at 3 °C. In the helix, protection from exchange is highest for the relatively inaccessible NHs of F30, K31, and A34 and weakest for the NHs of A29 and Q32. Of the solvent-accessible surface NHs in the helix (NH burial < 2.5 Å), only Y33 has a protection factor >10, with $P = 16$.

The magnitude of the highest protection factors obtained can be related to the binding affinity from the relationship derived by Paterson et al. (1990)

$$k_{free}/k_{bound,min} = ([G_{B2}\text{–IgG}]/K_d)^{1/2} \quad (4)$$

where [G_{B2}–IgG] ~ 0.27–0.55 mM. Thus, for maximum protection factors between 180 and 210 (Table 1), the association constant is calculated to be ~10^8 M^{-1} from eq 4. This value is consistent with association constants obtained from titration calorimetry which show that G_{B2} binds to intact rabbit IgG with a $K_a \sim 10^8$ M^{-1} (pH 7.6, 25 °C; Alexander et al., in preparation). The free energy of binding obtained from titration calorimetry (~2.7 kcal mol^{-1}) is consistent with the values of $\Delta\Delta G_{op}$ obtained for the most protected NHs (Alexander et al., in preparation). G_B can also bind weakly to the Fab fragment (Derrick & Wigley, 1992) with a $K_a \sim 3.5 \times 10^5$ M^{-1} (pH 7.0, 25 °C) (Alexander et al., in preparation). From eq 4, the highest predicted protection factor for Fab binding is only ~10–14. Therefore, the high protection factors obtained here are consistent with specific binding of G_{B2} to Fc rather than Fab.

DISCUSSION

Analysis of Exchange Rates in Free G_{B2}. Two principal models have been proposed for hydrogen exchange in proteins. The penetration model proposes that exchange can occur from the folded state of the protein with small-amplitude noncooperative fluctuations which allow access of hydrated catalyst to H-bonded NHs (Woodward & Hilton, 1980; Woodward

et al., 1982). In this model, the exchange mechanism is highly localized, and neighboring protons can have very different exchange rates and activation energies depending on their solvent accessibility [e.g., Goodman and Kim (1991)]. The local unfolding model states that H-bonded structure must open transiently for exchange with the hydrated catalyst to take place. Transient opening will involve cooperative units of structure or "unfoldons", the NHs of which will have similar exchange rates (Englander & Kallenbach, 1984; Mayne et al., 1992; Englander et al., 1992). In both models, H-bond breakage must occur for NH exchange to take place. Data supporting both models have been reported in the literature, and extensive reviews have appeared on the nature of the exchange mechanism [e.g., Woodward et al. (1982), Wagner (1983), Englander and Kallenbach (1984), and Englander and Mayne (1992)].

In view of the narrow range of exchange rates and ΔG_{op} values obtained in free G_{B2}, a cooperative exchange mechanism is likely for the majority of detectable NHs at 22 °C (Figure 3A). If this is the case, then NHs which require global unfolding of the protein for exchange to occur should have ΔG_{op} values which are consistent with the free energy of thermal unfolding, ΔG_u, extrapolated to the appropriate temperature. The unfolding reaction of G_{B2} has been examined using DSC and found to exhibit cooperative two-state behavior over a wide pH range with an unfolding transition near 80 °C at pH 7.0 (Alexander et al., 1992). The plot of ΔG_u vs temperature, calculated from thermal unfolding data using the Gibbs-Helmholtz equation, is a shallow parabola with a maximum at about 5 °C (Alexander et al., 1992). From this curve, the extrapolated values of ΔG_u at 22 and 3 °C are within experimental error of the ΔG_{op} values from NH exchange (Table 2). Therefore, the NH exchange data indicate that the majority of detectable NHs have free energies of opening which approximate the free energy of thermal unfolding. Thus, it appears that unfolding events for surface NHs such as K28 and Q32 are approximately as energetically costly as those for more buried NHs such as A34 and F52. This may in part be due to the efficient packing of the hydrophobic core of G_{B2} as well as the extensive network of H-bonds with a high percentage (~90%) of residues involved in H-bonding/secondary structure. In such a cooperative unit of structure, even local unfolding events may be energetically demanding and disrupt hydrophobic packing and H-bonding leading to larger amplitude global unfolding. Some parts of the H-bonded structure, such as L12, G14, T16, and T18 of the β2-strand, do not fall into the group of slow exchangers. These NHs apparently exchange without complete unfolding of the protein.

A number of possible sources of error may account for the discrepancy between ΔG_{op} values obtained by NMR and the calorimetric ΔG_u. These include extrapolation of the ΔG_u curve to low temperatures, measurement of exchange rates, calculation of intrinsic exchange rates, and possible overestimation of exchange rates in unfolded states of the protein. These latter rates are equated with the intrinsic exchange rates calculated for an unstructured peptide. However, the unfolded state may not be completely unstructured, in which case exchange rates would be slower than in a random coil peptide. This, in turn, would lead to an overestimation of ΔG_{op} (eq 3). The ΔG_{op} values for slow-exchange NHs in BPTI are similarly 1–1.5 kcal mol^{-1} higher than ΔG_u values obtained from extrapolation of thermal unfolding data (Roder, 1989). In addition, recent results on unligated and ligated staphylococcal nuclease show ΔG_{op} values 0.3–0.9 kcal mol^{-1} higher than ΔG_u determined from urea denaturation experiments (Loh et al., 1993). It is noteworthy that a more recent set of correction factors for intrinsic exchange rates (Bai et al., 1993) provides mean values of ΔG_{op} which are closer to the extrapolated calorimetric ΔG_u (Table 2).

A bound water molecule has been detected near the NHs of residues 32 and 33 in G_{B1}, and a bifurcated H-bond involving a bridging water molecule between 33NH and 29CO has been proposed (Clore & Gronenborn, 1992). While the exchange rate of 33NH is the fastest of the detectable NHs at 22 °C (Table 1), it is not fast in an absolute sense. This is perhaps not surprising since some NHs which H-bond to crystallographic water also have quite slow exchange rates (<0.4 h^{-1}) under similar conditions of pH and temperature (Mayne et al., 1992). As argued by Kim et al. (1993), slow exchange for some NHs H-bonded to water may be due to local rigidity which may constrain the NH in a low reactivity conformation. Hence, the NH of Y33 may exchange only when the protein undergoes large-amplitude unfolding. This idea is also consistent with a cooperative two-state unfolding model.

Exchange Mechanisms in Bound G_{B2}. The binding of IgG to G_{B2} results in a broadening of exchange rates (Figure 6) and ΔG_{op} values (Figure 3B) relative to free G_{B2}. The large range of protection factors indicates that exchange does not occur cooperatively for all detectable NHs in bound G_{B2}. Clearly, if all NHs exchanged by a global unfolding mechanism, then all P values would be equally high. Since some residues have small P values, localized unfolding of these residues can occur without greatly altering binding to IgG. This is most evident in the helix where a distinct boundary exists between weakly and strongly protected NHs at A29–F30 and K31–Q32 (Table 1). The highly protected NHs, which are mostly buried, constitute the slow-exchange core of bound G_{B2} (Figure 6) and most likely exchange by a cooperative global unfolding mechanism as in free G_{B2}. These residues probably make up the folding core of the bound protein (Woodward, 1993). In at least three other systems, BPTI (Roder & Wuthrich, 1986), cytochrome *c* (Roder et al., 1988), and lysozyme (Radford et al., 1992), the slowest exchanging NHs generally correspond to parts of the molecule which fold early as determined by quenched-flow methods.

The remaining NHs have small to intermediate protection factors. They are located at solvent-accessible positions in the helix, on the outer strands of the β-sheet, and at the ends of the inner β-strands. These NHs can probably exchange through more localized, smaller amplitude unfolding motions in the complex which do not require complete unfolding of the bound protein. While these locally unfolded states are still energetically costly, they do not greatly disrupt IgG binding. Globally unfolded states are not consistent with binding to IgG, however.

Implications of Protection Data with Respect to a Binding Surface. Of the nine most protected residues, six (L5, F30, A34, V39, F52, V54) have side chains buried in the hydrophobic core with a combined solvent-accessible surface area of ~8.5 Å^2. The other three (V6, K31, and T53) have surface side chains. Peptide mapping (Frick et al., 1992) and chemical shift perturbation studies (Gronenborn & Clore, 1993) indicate that the helix, part of L3, and the β3-strand form the binding surface. Residues V6 and T53 are removed from this putative binding site while the side chain of K31 contributes ~100 Å^2 to the solvent-accessible surface and is a potential contact residue. The side chain of K31 is proximal to the indole ring of W43 (Figure 8), which has also been implicated in the binding surface (Gronenborn & Clore, 1993).

No protection factor could be determined for W43 due to its fast exchange. From crystallography, about 1000 Å^2 of solvent-accessible surface area is covered in the protein A–Fc complex, with mostly hydrophobic interactions between side chains stabilizing the complex (Deisenhofer, 1981). If a similar binding area exists for the protein G–Fc complex, then a number of other contacts involving side chains must also be present. It should be noted that, since total human IgG was used in this study, the protection factor map represents the average of binding to all four subclasses.

Based on a comparison of our results with other studies on the mode of IgG binding to protein G (Frick et al., 1992; Gronenborn & Clore, 1993), the protected NHs of residues F30, K31, A34, and V39 are likely buried at the binding interface. In contrast, the strongly protected NHs in the β1- and β4-strands (L5, V6, F52, T53, and V54) are removed from the putative binding interface. The latter group of NHs could be highly protected due to IgG contact with side chains from the β3-strand, although the β3-NHs are not strongly protected themselves. Alternatively, the exchange rates of the strongly protected β1- and β4-NHs may be indirectly slowed through long-range interactions between nonpolar side chains in the helix and β-sheet. The side chains of L5, F30, A34, V39, F52, and V54 are buried and have extensive van der Waals contacts with each other (Figure 8). These interactions form the basis of the well-packed hydrophobic core of the protein. The effect of constraining the opening motions which lead to exchange of one of these hydrophobic residues by IgG binding may also constrain opening motions which result in exchange of other close contact hydrophobic residues through cooperative effects.

The opening motions of either the H-bond donor or H-bond acceptor, or both, may affect the degree of protection. For example, although the side chain of V6 is not involved in the hydrophobic core, its NH is highly protected from exchange in the complex. The H-bond acceptor is F52CO, and the F52 aromatic side chain is involved in a number of close contacts in the hydrophobic core. Antibody binding may constrain opening motions which lead to solvent exposure of side chains in the hydrophobic core. This, in turn, may limit fluctuations of the H-bond acceptor for V6NH, leading to strong protection of V6NH. Slowed exchange of F30, A34, and V39 may be partly due to the H-bonding between these residues where the donor–acceptor pairs are V39NH–A34CO and A34NH–F30CO.

Long-range effects have been reported recently in a complex between hen egg lysozyme and the HyHEL-5 antibody (Benjamin et al., 1992), but while the remote and boundary NHs were significantly protected (P = 1.9–13), their protection factors were still much less than for contact residues (P = 44–65). This is in contrast to the results presented here, where some of the more distant NHs are protected from exchange to the same extent as NHs that are putatively buried at the binding interface. This may be partly due to the small size and highly cooperative nature of the G_{B2} structure whereby no residues are truly "remote" from the binding interface. Slowed exchange of NHs outside the structural epitope has also been observed in antibody complexes with cytochrome *c* (Mayne et al., 1992).

H–D Exchange at the Binding Interface. Detectable surface NHs do not appear to be highly protected in these studies (Figure 9). This indicates that considerable exchange is occurring at the putative binding interface and that the interfacial region is accessible to solvent (Benjamin et al., 1992; Bhat et al., 1993). Transient partial exposure of the binding interface to solvent without dissociation of the complex may allow contact surface NHs to exchange by a localized unfolding mechanism whereas larger amplitude global opening motions required for exchange of core NHs would still be more restricted. This is a possible explanation for why surface NHs at the putative binding interface are not as strongly protected as some buried NHs.

Benjamin et al. (1992) also proposed a transient exposure of the binding interface to solvent to account for the lower than expected protection factors observed for contact and buried NHs in the complex between hen egg lysozyme and the HyHEL-5 antibody. Our results differ from those in that, while surface NHs are not strongly protected, NHs buried at the putative binding interface have the expected protection factors for a complex with $K_a \sim 10^8$ M^{-1}.

CONCLUSIONS

The measurement of exchange rates in free and IgG-bound G_{B2} provides insight into the mechanisms governing NH exchange and folding. In free G_{B2}, 28 of the slowest exchanging NHs have rates which are clustered within an order of magnitude. This reflects the highly cooperative nature of the G_B structure whereby the free energy of opening approximates the free energy of thermal unfolding for the majority of detectable NHs. In bound G_{B2}, NH exchange is less cooperative, and local and global unfolding events can be readily differentiated. IgG binding may affect the conformational dynamics of G_{B2} since some distant residues have protection factors as high as residues buried at the putative binding interface. For this reason, the IgG binding site cannot be unambiguously determined from the protection pattern obtained in this study.

The slow-exchange core NHs in bound G_{B2} likely unfold as a cooperative unit since they all have high protection factors. Thus, the rigid slow-exchange core probably corresponds with the folding core of the bound protein. Residues with intermediate protection factors, such as A26 and Y33, are situated further out from the slow-exchange core, and the smallest protection factor residues are near the surface or at the ends of β-strands. These residues can exchange by more localized unfolding mechanisms such that their unfolded states are still consistent with IgG binding to some extent. Unfolding of the slow-exchange core is not consistent with IgG binding, however.

ACKNOWLEDGMENT

We thank Drs. John Moult and Krzysztof Fidelis for the solvent-accessibility calculations and Dr. Travis Gallagher for advice on the use of molecular graphics programs. We also thank Drs. Travis Gallagher, John Moult, and Roberto Poljak for helpful discussions.

SUPPLEMENTARY MATERIAL AVAILABLE

Table of exchange rates and protection factors obtained for individual NOESY cross-peaks at 3 and 22 °C (5 pages). Ordering information is given on any current masthead page.

REFERENCES

Akerstrom, B., & Bjorck, L. (1986) *J. Biol. Chem. 261*, 10240–10247.

Alexander, P., Fahnestock, S., Lee, T., Orban, J., & Bryan, P. (1992) *Biochemistry 31*, 3597–3603.

Bai, Y., Milne, J. S., Mayne, L., & Englander, S. W. (1993) *Proteins 17*, 75–86.

Benjamin, D. C., Williams, D. C., Jr., Smith-Gill, S. J., & Rule, G. S. (1992) *Biochemistry 31*, 9539–9545.
Bhat, T. N., Bentley, G. A., Boulot, G., Greene, M. I., Tello, D., Dall'Acqua, W., Souchon, H., Schwarz, F. P., Mariuzza, R. A., & Poljak, R. J. (1994) *Proc. Natl. Acad. Sci. U.S.A. 91*, 1089–1093.
Brandt, P., & Woodward, C. K. (1987) *Biochemistry 26*, 3156–3162.
Chothia, C. (1976) *J. Mol. Biol. 105*, 1–14.
Clore, G. M., & Gronenborn, A. M. (1992) *J. Mol. Biol. 223*, 853–856.
Covington, A. K., Robinson, R. A., & Bates, R. G. (1966) *J. Phys. Chem. 70*, 3820–3824.
Deisenhofer, J. (1981) *Biochemistry 20*, 2361–2370.
Derrick, J. P., & Wigley, D. B. (1992) *Nature 359*, 752–754.
Englander, J. J., Calhoun, D. B., & Englander, S. W. (1979) *Anal. Biochem. 92*, 517–524.
Englander, S. W., & Kallenbach, N. R. (1984) *Q. Rev. Biophys. 16*, 521–655.
Englander, S. W., & Mayne, L. (1992) *Annu. Rev. Biophys. Biomol. Struct. 21*, 243–265.
Englander, S. W., Englander, J. J., McKinnie, R. E., Ackers, G. K., Turner, G. J., Westrick, J. A., & Gill, S. J. (1992) *Science 256*, 1684–1687.
Fahnestock, S. R., Alexander, P., Nagle, J., & Filpula, D. (1986) *J. Bacteriol. 167*, 870–880.
Frick, I. M., Wikstrom, M., Forsen, S., Drakenberg, T., Gomi, H., Sjobring, U., & Bjorck, L. (1992) *Proc. Natl. Acad. Sci. U.S.A. 89*, 8532–8536.
Goodman, E. M., & Kim, P. S. (1991) *Biochemistry 30*, 11615–11620.
Gouda, H., Torigoe, H., Saito, A., Sato, M., Arata, Y., & Shimada, I. (1992) *Biochemistry 31*, 9665–9672.
Gronenborn, A. M., & Clore, G. M. (1993) *J. Mol. Biol. 233*, 331–335.
Gronenborn, A. M., Filpula, D. R., Essig, N. Z., Achari, A., Whitlow, M., Wingfield, P. T., & Clore, G. M. (1991) *Science 253*, 657–661.
Hvidt, A., & Nielsen, S. O. (1966) *Adv. Protein Chem. 21*, 287–386.
Jeener, J., Meier, B. H., Bachmann, P., & Ernst, R. R. (1979) *J. Chem. Phys. 71*, 4546–4553.
Kim, K.-S., Fuchs, J. A., & Woodward, C. K. (1993) *Biochemistry 32*, 9600–9608.
Kraulis, P. J. (1991) *J. Appl. Crystallogr. 24*, 946–950.
Kumar, A., Ernst, R. R., & Wuthrich, K. (1980) *Biochem. Biophys. Res. Commun. 95*, 1–6.
Lian, L.-Y., Yang, J. C., Derrick, J. P., Sutcliffe, M. J., Roberts, G. C. K., Murphy, J. P., Goward, C. R., & Atkinson, T. (1991) *Biochemistry 30*, 5335–5340.
Lian, L.-Y., Derrick, J. P., Sutcliffe, M. J., Yang, J. C., & Roberts, G. C. K. (1992) *J. Mol. Biol. 228*, 1219–1234.
Loh, S. N., Prehoda, K. E., Wang, J., & Markley, J. L. (1993) *Biochemistry 32*, 11022–11028.
Macura, S., Huang, Y., Suter, D., & Ernst, R. R. (1981) *J. Magn. Reson. 43*, 259–281.
Mayne, L., Paterson, Y., Cerasoli, D., & Englander, S. W. (1992) *Biochemistry 31*, 10678–10685.
Molday, R. S., Englander, S. W., & Kallen, R. G. (1972) *Biochemistry 11*, 150–157.
Moult, J., Sussman, F., & James, M. N. G. (1985) *J. Mol. Biol. 182*, 555–566.
Myhre, E. B., & Kronvall, G. (1977) *Infect. Immun. 17*, 475–482.
Orban, J., Alexander, P., & Bryan, P. (1992) *Biochemistry 31*, 3604–3611.
Otting, G., Widmer, H., Wagner, G., & Wuthrich, K. (1985) *J. Magn. Reson. 66*, 187–193.
Paterson, Y., Englander, S. W., & Roder, H. (1990) *Science 249*, 755–759.
Radford, S. E., Dobson, C. M., & Evans, P. A. (1992) *Nature 358*, 302–307.
Reis, K. J., Ayoub, E. M., & Boyle, M. D. P. (1984) *J. Immunol. 132*, 3098–3102.
Robertson, A. D., & Baldwin, R. L. (1991) *Biochemistry 30*, 9907–9914.
Roder, H. (1989) *Methods Enzymol. 176*, 446–473.
Roder, H., & Wuthrich, K. (1986) *Proteins: Struct., Funct., Genet. 1*, 34–42.
Roder, H., Wagner, G., & Wuthrich, K. (1985) *Biochemistry 24*, 7407–7411.
Roder, H., Elove, G., & Englander, S. W. (1988) *Nature 335*, 700–704.
States, D. J., Haberkorn, R. A., & Ruben, D. J. (1982) *J. Magn. Reson. 48*, 286–292.
Stone, G. S., Sjobring, U., Bjorck, L., Sjoquist, J., Barber, C. V., & Nardella, F. A. (1989) *J. Immunol. 143*, 565–573.
Wagner, G. (1983) *Q. Rev. Biophys. 16*, 1–57.
Werner, M. H., & Wemmer, D. E. (1992) *J. Mol. Biol. 225*, 873–889.
Woodward, C. (1993) *Trends Biochem. Sci. 18*, 359–360.
Woodward, C. K., & Hilton, B. D. (1980) *Biophys. J. 32*, 561–575.
Woodward, C., Simon, I., & Tuchsen, E. (1982) *Mol. Cell. Biochem. 48*, 135–160.
Wright, C., Willan, K., Sjodahl, J., Burton, D. R., & Dwek, R. (1977) *J. Biochem. 167*, 661–668.
Wuthrich, K. (1986) *NMR of Proteins and Nucleic Acids*, Wiley, New York.
Zinn-Justin, S., Roumestand, C., Drevet, P., Menez, A., & Toma, F. (1993) *Biochemistry 32*, 6884–6891.